UNIVERSITY OF CALIFORNIA SAN DIEGO

Biophysical characteristics of NFkappaB-IkappaBalpha's Intrinsically Disordered Regions

A Thesis submitted in partial satisfaction of the requirements.
for the degree Master of Science

in

Chemistry

by

Luis Oliva

Committee in charge:

Professor Elizabeth A. Komives Chair
Professor Lisa M. Jones
Professor Brian Leigh

2024

The Thesis of Luis Oliva is approved, and it is acceptable in quality and form for publication on microfilm and electronically.

University of California San Diego

2024

DEDICATION

This thesis is dedicated to my friends, my community, and above all my family. The friends I have made along the way, through classes, through the jobs I worked, and throughout all my experiences, I thank you so much for your support. I hope to make the best of this journey and contribute towards increasing inclusion, equity, and accessibility to higher education, and making science fun for students of all backgrounds.

TABLE OF CONTENTS

LIST OF FIGURES

LIST OF TABLES

ACKNOWLEDGEMENTS

I would like to acknowledge Professor Elizabeth A. Komives, as chair of the committee, Professors Brian Leigh, and Lisa M. Jones as my committee members. Their guidance has been essential to my journey. Thank You!

Chapter 1, 2, 3, and 4 are currently being prepared for submission for publication of the material. Oliva, Luis. This thesis author was the primary investigator and author of this material with Professor Elizabeth A. Komives.

ABSTRACT OF THE THESIS

Biophysical characteristics of NFkappaB-IkappaBalpha's Intrinsically Disordered Regions

by

Luis Oliva

Master of Science in Chemistry

University of California San Diego, 2024

Professor Elizabeth A. Komives Chair

In this study we characterized the NFkB-IkBa interaction with a focus on intrinsically disordered regions (IDRs). We combined FPOP-MS to probe side chain protection with HDX-MS to probe backbone protection which may be occurring in IDR interactions. FPOP-MS captured IκBα's AR5 and AR6 were highly oxidized under apo conditions but protected when bound to NFkB. HDX-MS also showed folding of this region upon NFkB binding. The intrinsically disordered N-terminal domain, also known as the signal recognition domain (SRD), of IκBα

exhibits protection occurring at the side chains, but not in the backbone. This protection occurs at regions near IκBα's phosphorylation sites S32 and S36. A region of the NFκB's transcription activation domain (TAD) near IκBα's SRD according to a structural model exhibited protection at the side chains, but not the backbone. The results of this study suggest NFκB's TAD and IκBα's SRD form a fuzzy complex that may affect SRD regulation.

Chapter 1 Introduction: Why Characterize NFkappaB and IkappaBalpha’s IDRs?

NFκB plays a vital role in protein interaction networks involved in our immune system (Fig. 1A, B). Our understanding of their biophysical characteristics is limited due to the lack of studies performed focusing on their intrinsically disordered regions (IDRs). Protein disorder is a phenomenon observed in proteins involved in a diverse range of pathways due to their ability to take on various conformations. Previous studies have observed that dysregulation of intrinsically disordered proteins can give rise to disease. Dysregulation of this family of proteins has been linked to hyper-inflammation which may result in development of neuroinflammation, cancer, and/or autoimmunity. It is important to characterize the role of intrinsically disordered regions (IDRs) found in proteins such NFκB , to have a thorough understanding of the biophysical characteristics of these transcription factors and their inhibitors.

1.1 Role of NFκB in Immunity: Inflammation

The Nuclear Factor-kB (NFκB) is a family of transcription factors which regulate a broad set of genes associated with the immune system and inflammatory responses. This family of proteins is composed of p50, p52, RelA (also known as p65), RelB, and c-Rel which can form hetero-homodimers between each other and bind to specific DNA sites (Liu, Zhang et al. 2017). Activation of this system is understood to be induced by various receptor-mediated signaling pathways. Inactive NFκB is maintained in the cytoplasm by IκBα; in fact, this (Dixit and Mak 2002). While bound to IκBα, NFκB is unable to bind DNA, so removal of this inhibitor is required upon activation. IκBα is removed from NFκB when IκBα is phosphorylated and recognized by the Beta-TrCP component of the SCF ubiquitination complex. Upon IκBα's degradation, NFκB is released and translocated into the nucleus in the classical signaling pathway. The classical signaling pathway is triggered by a broad variety of stimuli such as

cytokine receptors, pattern-recognition receptors, TNF receptor (TNFR) superfamily members, T cell receptors and B cell receptors. In addition to the classical signaling pathway, there are also nonclassical NFκB activation mechanisms. Nonclassical NFκB pathways respond to specific stimuli such as ligands of specific TNFR subfamilies, in particular LTBR, BAFFR, CD40 and RANK. In the nonclassical signaling pathway, p100 is phosphorylated by IKKa and processed to form p52. IKKa is activated by NIK. This non-classical NIK/IKKa/p52 pathway is understood to be triggered by the activation of lymphotoxin B receptor (LTBR) in stromal nonlymphoid cells (Davis, Hatzubai et al. 2002). Once activated, NFκB plays a pivotal role in inflammation regulation beyond its involvement in pro-inflammatory gene expression in immune cells. In fact, NFκB can also regulate T cell differentiation and effector functions. Inflammatory gene induction is a protective line of defense the human body utilizes against infection and tissue damage; however, dysregulation of this system can lead to diseases relating to chronic inflammation (Figure 1A).

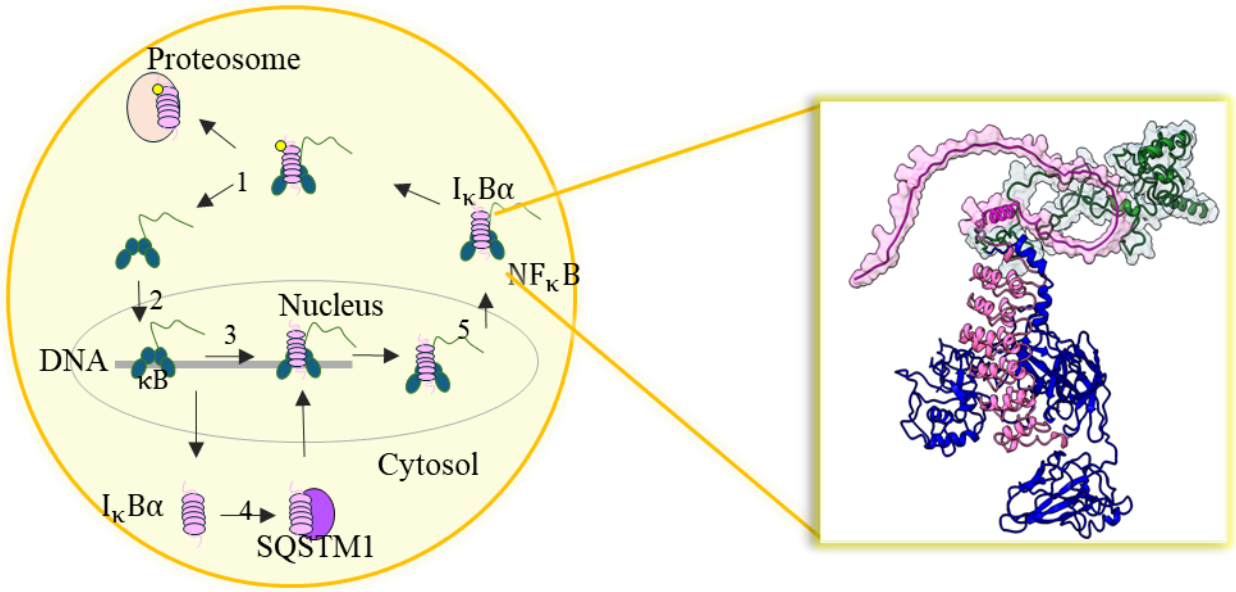

Figure 1 **NFκB activates the inflammation response.**

B) The most abundant NFκB complex responsible for rapid response to inflammatory signals is the RelA-p50. 1) Upon phosphorylation IκBα is degraded via proteasomal degradation, releasing NFκB. 2) NFκB is translocated into the nucleus where it binds to DNA. 3) NFκB is responsible for activation of inflammatory genes and transcribes more of its own inhibitor. 4) When IκBα is made, it is believed to bind to SQSTM1 to be translocated into the nucleus. 5) IκBα facilitates dissociation of NFκB from DNA and the NFκB-IκBα complex is exported. 6) NFκB-IκBα remain in the cytoplasm until NFκB is activated again.

Chronic inflammation can present itself through various physiological symptoms such as neuroinflammation, autoimmunity, and/or cancer (Figure 2). NFκB is a key regulator of inflammation and apoptosis which is found to be involved in systemic aging and pathogenesis of many neurodegenerative diseases. Increased concentrations of RelA being translocated into the nucleus has been observed in patients with Parkinson's Disease (PD). Various pathways involved in neuroinflammation, impaired autophagy, and oxidative stress have been found to contribute to PD pathogenesis, many of which can be linked to being regulated by NFκB (Bellucci, Bubacco et al. 2020). The pathogenesis of autoimmunity disorders such as type I diabetes, rheumatoid arthritis, multiple sclerosis, systemic lupus erythematosus, and inflammatory bowel disease have all been previously linked to NFκB 's activity (Bellucci, Bubacco et al. 2020). NFκB 's regulation of chemokines expression is known to enhance tumorigenesis and metastasis in cancer patients (Taniguchi and Karin 2018). NFκB is interlaced in various pathways that must be precisely regulated to maintain homeostasis, and thus its characterization may provide insight into fundamental biophysical properties that help maintain a strict immune response.

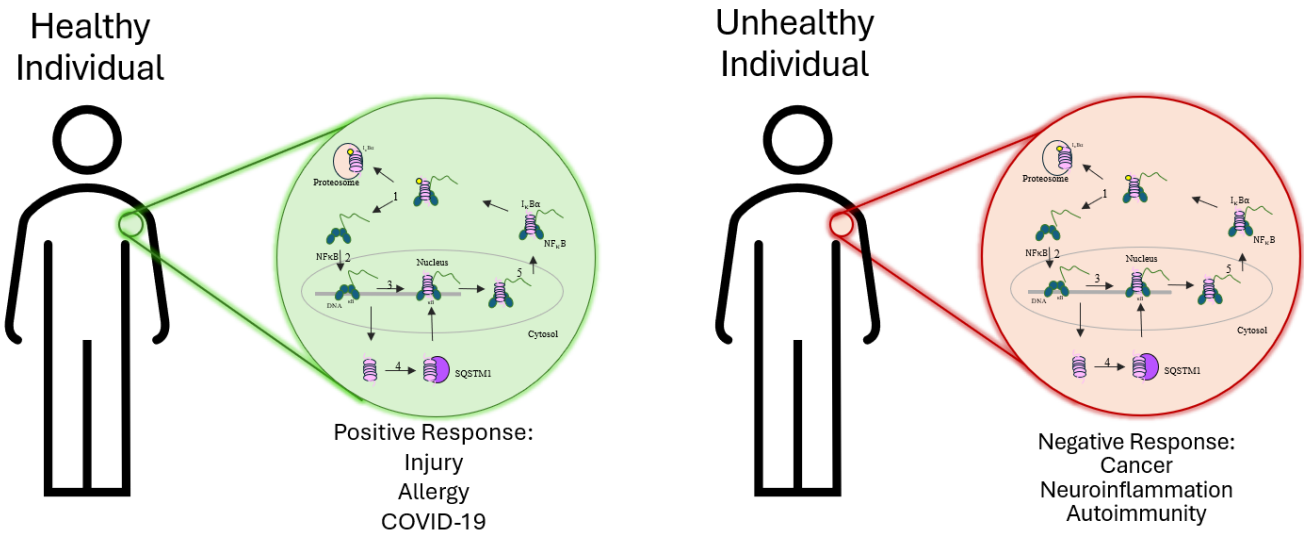

Figure 2 NFκB 's activity is crucial to our immune response.

It can also lead to detrimental effects. To the left a healthy individual is illustrated with a list of potential responses of NFκB to its immune system as a result of injury, allergy or viral infection. To the right an unhealthy individual is illustrated in which NFκB activity can have negative impacts on an someone's health. A list of unhealthy responses are listed under the unhealthy individual that can arise from NFκB dysregulation such as cancer, neuroinflammation, and autoimmunity.

1.2 IDRs in the NFκB /IkB Family

Many signaling pathways require proteins to exhibit unique characteristics that can constitute specific signaling cascades. In fact, IDRs allow proteins the versatility to take on various configurations, each of which correspond to specific functions. IDRs don't fold into stable secondary structures independently; however, some can transition from disordered-to-ordered when bound to specific substrates or triggered by post translational modifications (PTMs). For instance, TADs are found to be predominantly disordered, which allows for them to interact with multiple transcription co-activators/repressors, but they may become ordered upon binding. This phenomenon is observed in p65's interaction with CBP via its TA1 domain which forms an alpha helix upon binding (Lecoq, Raiola et al. 2017). IκBα's AR5 and AR6 fold upon binding to

NFκB (Sue, Cervantes et al. 2008) (Figure 4). This phenomenon allows the protein to inhibit the NFκB complex and protects its degron region from being recognized for proteolytic degradation. IDRs can also remain disordered when bound and serve the purpose of amplifying allosteric regulation. These attributes all enable protein interaction networks to remain precisely controlled by allowing their interactions/PTMs to be reversible. Thus, it is important to better characterize IDRs of signaling molecules rather than only focusing on the domains with secondary structures.

1.3 Protein Topology

Proteins are biomolecules composed of multiple and/or single polypeptide chains in which amino acids serve as building blocks. Amino acids (AA) are joined through a peptide bond that links the carboxylic acid group of an AA group to another (usually limited to the 20 naturally occurring AAs). Protein topology can be deconstructed to four orders of protein structure. Primary structure refers to the sequence of the amino acids that make up a polypeptide chain. This sequence is read from the N-terminus (the AA with a free amine group) to the C-terminus (the AA with a free carboxyl group). The secondary structure refers to the local structure of a protein that arises from intramolecular interactions occurring between backbone atoms of the polypeptide. These interactions can create two dimensional structures known as alpha helix or beta pleated sheets. The tertiary structure is recognized as the three-dimensional architecture of a single polypeptide that arises from the secondary structure folding upon itself (during a process known as protein folding). Protein folding is guided by the interactions formed between the secondary structures, which usually happens through side chain interactions (via hydrogen bonding, ionic bonding, dipole-dipole interactions, and London dispersion forces). The highest

order of protein structure is the quaternary structure which arises from multiple polypeptide chains interacting which each other. While some proteins can take on stable structures such as alpha helix and beta sheets, IDPs can exhibit dynamic configurations that can vary from completely unstructured to partially structured, which may be seen as random coils, molten globule-like aggregates or flexible linkers.

Complex biomolecules such as IDPs can take on various conformations that correspond to unique functions guided by binding partners and/or PTMs. IDPs' conformational diversity leads them to have a complex multi-funnel thermodynamic landscape in which they don't reach a minimal energy level. Identifying specific conformations to corresponding functions of IDPs is key to deciphering their biophysical characteristics at varying points in signaling networks.

A conventional method used to theoretically understand protein interactions is by analyzing the minimally and highly frustrated contacts during protein interactions. Protein frustration can be defined as a physical phenomenon that occurs when proteins are unable to reach a minimum energy level because of geometric reasons, or competition between interactions from different entities (e.g. DNA, multiple amino acids, substrates, etc.). The development of the Energy Landscape Theory of protein folding opened a new avenue through which we can study and understand residual frustration in macromolecules (Röder and Wales 2018). To properly fold, proteins must follow physical constraints and satisfy local interactions altogether, which can give rise to either high or minimal frustration index scores. IDPs exhibit high frustration index scores due to their inability to reach a minimal energy level and instead remain in a higher energy state. Computational/statistical local frustration analyses can be leveraged to provide insight on interactions between intrinsically disordered proteins that may not be captured via experimental

approaches due to experimental limitations. Further explanations regarding the fundamental concepts and mathematical explanations of minimal frustration can be found in Chapter 4.

1.4 Introduction Summary

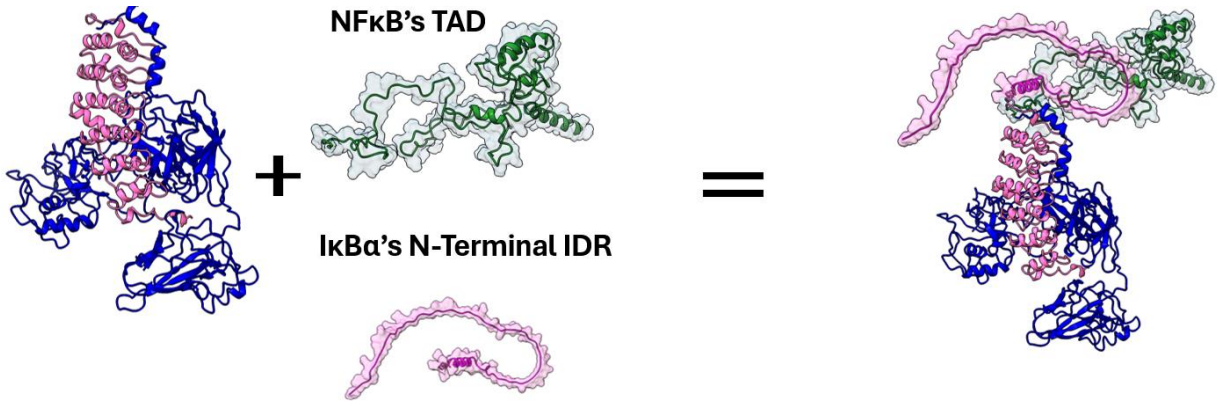

Figure 3 NFκB -IκBα Structural Studies

Previously structural studies didn't contain the intrinsically disordered regions (IDRs) of NFκB and IκBα. In this study the N-terminal IDR of IκBα and the C-terminal IDR of NFκB (the 230 aa transcription activation domain: TAD) are present. NFκB can be seen in blue, while its TAD is in green. IκBα is displayed in pink.

Previous studies conducted on NFκB -IκBα excluded their intrinsically disordered regions which are crucial to their function. NFκB 's TAD has been found to be important for DNA binding. Meanwhile, IκBα's intrinsically disordered N-terminus contains two phosphorylation sites (S32 and S36) that are a necessary step for its degradation and release of NFκB . In this thesis, *in vitro* and *in silico* studies are presented to characterize NFκB -IκBα interactions. Previous studies failed to address potential roles of IκBα's and NFκB 's IDRs. To biophysically characterize NFκB -IκBα IDRs *in vitro* HDX-MS and FPOP-MS analysis was conducted and followed up by *in silico* frustration analysis using Frustratometer to generate localized frustrated contacts.

Chapter 2 HDX MS: NFkappaB ’s C-Terminus and IkappaBalpha’s N-Terminus Remain Disordered Upon Binding

2.1 HDX-MS Background

Hydrogen deuterium exchange was initially developed in the field of NMR spectroscopy to study molecular dynamics; however, mass spectrometry has allowed this reaction to be leveraged to study supra-macromolecular structures. By coupling the reactivity of hydrogen deuterium exchange with mass spectrometry, we can provide peptide level resolution of protein structure and dynamics. This method takes advantage of the naturally occurring exchange between deuterons ($^2H^+$ or D^+) when diluting a protein complex in a D_2O buffer (prepared with the same components as the buffer the protein was previously in at neutral pH). This phenomenon allows structural biologists to determine the regions of a protein that tightly sequester amide hydrogens vs the regions that exhibit highly exposed amide hydrogens. When proteins form secondary structures, this is achieved through hydrogen bonding between amino acids, while if the regions are disordered, the hydrogens remain accessible. When proteins bind to other proteins, they can also cover and protect each other's surfaces. Thus, structural biologists can use this method to determine the structural rigidity of a protein under varying conditions.

2.2 Materia Methods

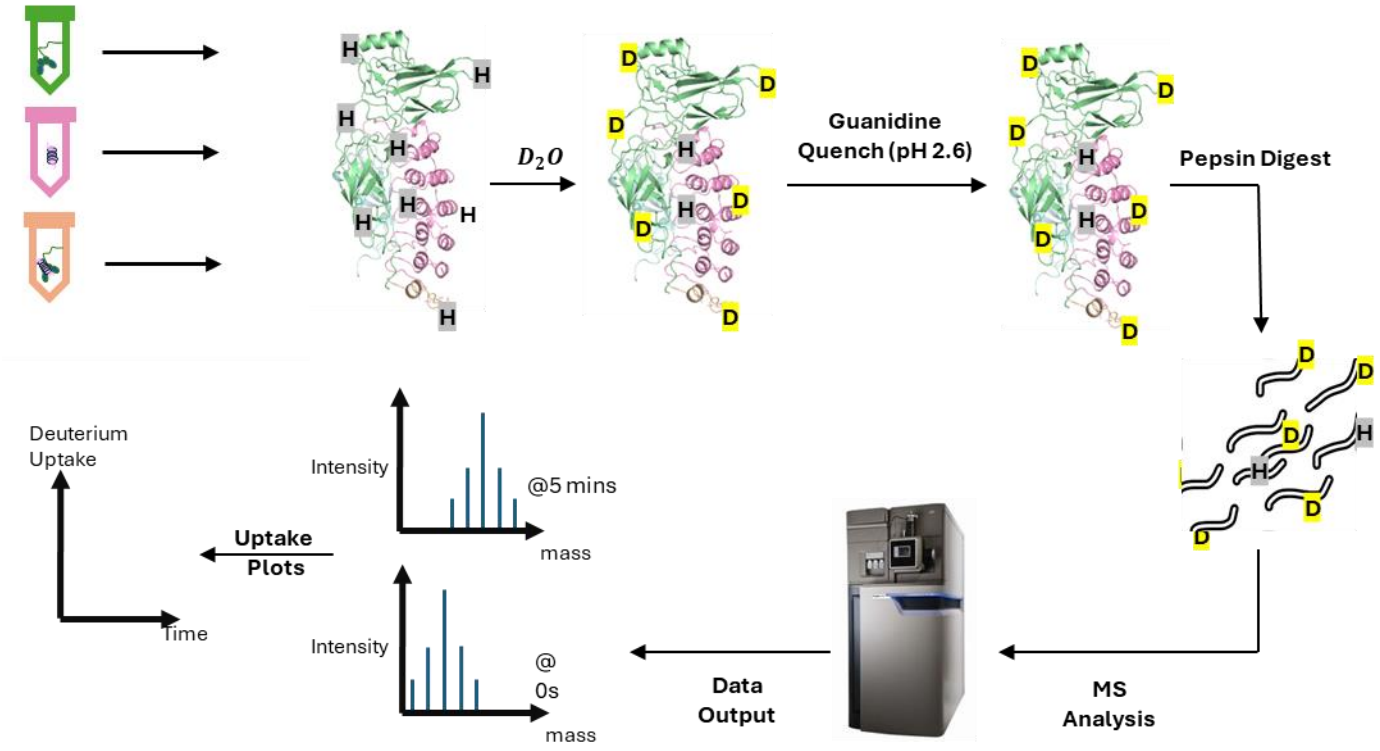

Figure 4 Sample preparation for HDX-MS

This starts by obtaining the systems in the appropriate conditions. The unbound and bound proteins are separately incubated in D2O buffer and quenched and digested at pH 2.5. A Synapt 2G-Si is then used to analyze deuterated peptides. Data is then processed using DynamX.

2.2.1 Protein Purification

N-terminal hexahistidine murine $p50_{39-350}/RelA_{19-549}$ (hereafter referred to as $NFkB_{FL}$), $p50_{39-350}/RelA_{19-321}$ (hereafter referred to as $NFkB_{RHD}$), and $IkB\alpha_{2-317}$ were expressed using a modified pET 22b vector containing corresponding genes. All vectors were transformed into E. coli BL-21 (DE3) cells. Cells were grown to an A_{600} of 0.6 at 37 ˚C in M9 minimal media with ampicillin antibiotic selection, followed by a 20 min incubation period on ice. Protein expression was induced using 0.2 M IPTG and incubated overnight at 18 ˚C. Cells were harvested via centrifugation and supernatant was discarded. $NFkB_{FL}$, $NFkB_{RHD}$, and

$IkB\alpha_{2-317}$ pellets were sonicated and purified by Ni^{2+}-NTA chromatography followed by dialysis, followed by cation exchange chromatography (MonoS; GE healthcare), and a size exclusion chromatography. All purification chromatography steps were performed at 4 ˚C as previously described (Baughman, Narang et al. 2022).

2.2.2 Hydrogen-Deuterium Exchange Mass Spectrometry.

HDX-MS was performed using automated LEAP HDX technology coupled with a Synapt G2Si. H_2O and D_2O buffers were made with phosphate buffer containing 50mM Phosphate and 150mM NaCl, lyophilized and resuspended D_2O to prepare the D_2O buffer and milipore water for the H_2O buffer. $NF\kappa B_{FL}, NF\kappa B_{RHD},\ NF\kappa B_{FL} - I\kappa B\alpha, and\ I\kappa B\alpha - NF\kappa B_{RHD}$ stocks were prepared at 5 μM and a 4 μL volume was incubated for 5 minutes at room temperature (25 ˚C) followed by being mixed with 56 μL of H_2O buffer as a negative control, and D_2O buffer for the time points of 0, 0.5 min, 1 min, 2 min, 5 min at RT. It has been previously validated that these times and temperatures best capture allosteric transitions. The HDX reaction is quenched with 60 μL of 250 mM Guanadine, pH 2.5 at 0˚C. After the quenched HDX reaction is homogenous, 50 μL volume was injected into a fluidic system containing an in-line pepsin column (Immobilized pepsin, Pierce Inc,) at 15˚C followed by a BEH C18 Vanguard pre-column and separated by analytical chromatography (Acquity UPLC BEH C18, 1.7 μM, 1.0 x 50 mm, Waters Corporation) with an acetonitrile gradient of 7-85% acetonitrile in 0.1% formic acid over 7.5 minutes at a flow rate of 40 μL/min. Peptides were then treated with electrospray ionization and analyzed with a Water Synapt GSi quadrupole time-time-of-flight mass spectrometer. The acquisition parameters were as follows: data collection in mobility, ESI+ mode, mass range of 200-2,000 (m/z), scan time of 0.4 seconds. Leu-enkephalin was used for lock mass correction,

which was infused in 30 second intervals. MS^e was used for data collection. All processes were repeated in triplicates, for a protein concentration of 5 μM protein. A minimum number 250 ion counts for low energy peptide was applied as well as 50 ion counts was applied for fragmented ions.

2.2.3 Data Processing

Mass spectrometry data was processed using PLGS and DynamX 3.0 (Waters Corporation) subsequently to identify the peptides of interest. The following filtering parameters were applied to the data; cut off score of 7.0, error tolerance of 5 ppm and peptide must be identified in 2 of 3 identification runs. Deuterium uptake calculations were determined using the centroids of the mass envelopes of the envelopes of the deuterated samples compared to the corresponding peptide in the undertreated control. This process was executed for three technical replicates. Global back exchange correction factors were determined from the average percent exchange detected in disordered region. The data presented here is the mean values of back (+/-) SEM of three technical replicates after global back exchange corrections were made.

2.3 Results

To characterize the intrinsically disordered N-terminus of IκBα as well as the intrinsically disordered C-terminus of NFκB apo vs bound, HDX-MS was performed at RT (~ 25 ˚C). I hypothesized that dynamic interactions and/or structural information of the intrinsically disordered regions may be captured by HDX-MS experiments. The experiment would also serve to refute previous claims of IκBα's N-terminus taking on a secondary structure upon binding to NFκB as determined by computational approaches (Röder and Wales 2018). IκBα, $NFkB_{RHD}$,

$NFkB_{FL}$, IκBα- $NFkB_{RHD}$ and IκBα- $NFkB_{FL}$ were incubated with D_2O buffer for varying time points ranging from 0 seconds to 5 minutes and the reaction was stopped by the addition of Guanidine quench. The data presented in figure 6 and 7 can be referenced to demonstrate information obtained from HDX-MS.

Figure 5 Protein sequence coverage of IκBα.

The amino acid sequence of the hexahistidine-TEV cleavage site – IκBα of this protein is illustrated above. The green blocks below the sequence represent the peptides produced by a pepsin protease digest.

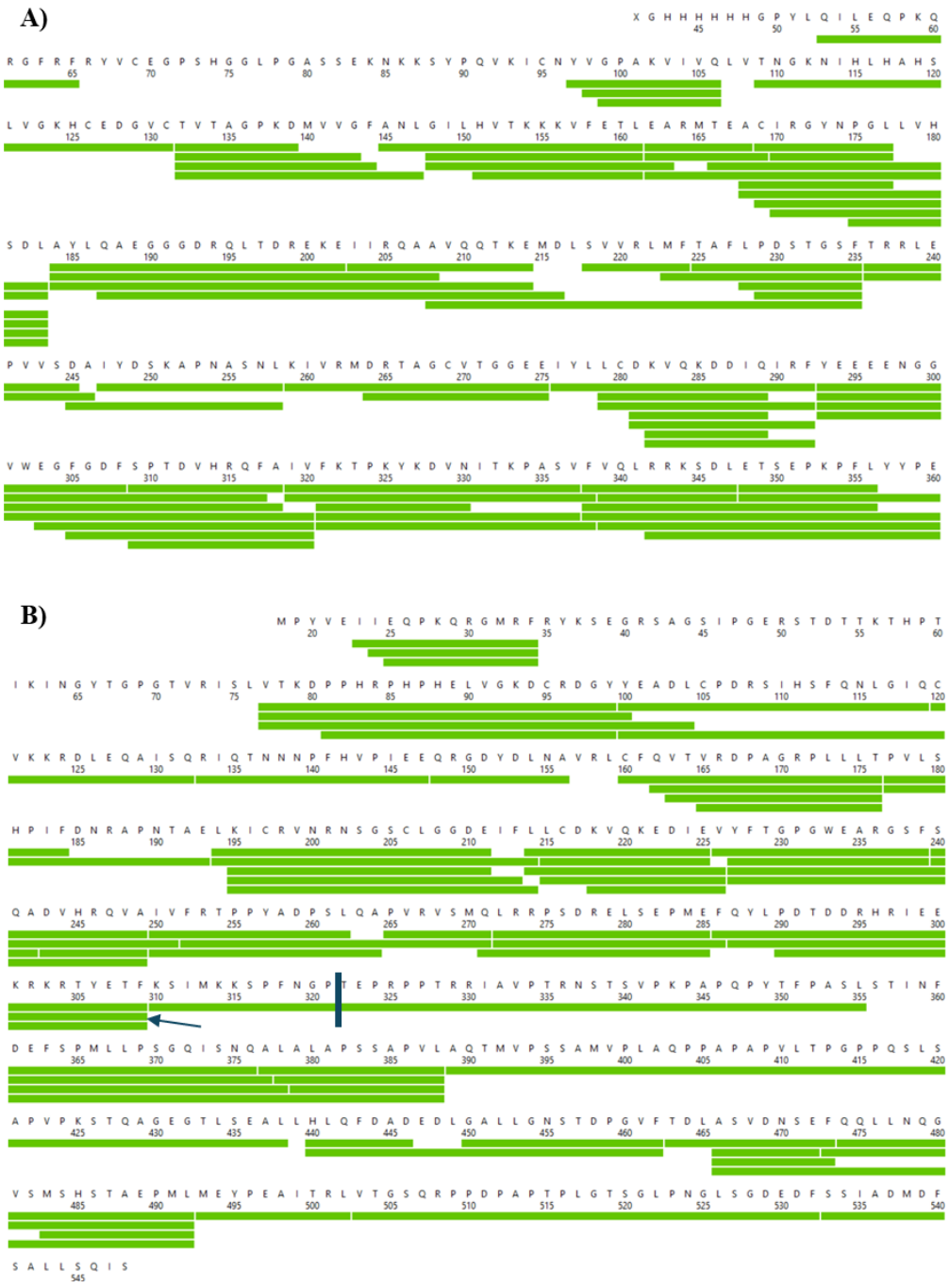

Figure 6 Protein sequence coverage of NFκB A) p50 and B) p65

Sequences are written out with green blocks below to represent the peptide products from a pepsin digested. A blue line is used to demonstrate where the sequence will of $NFkB_{RHD}$p65 is truncated. The arrow pointing to the peptides that ends at residue 310 of p65 represents the last peptide used for $NFkB_{RHD}$ p65.

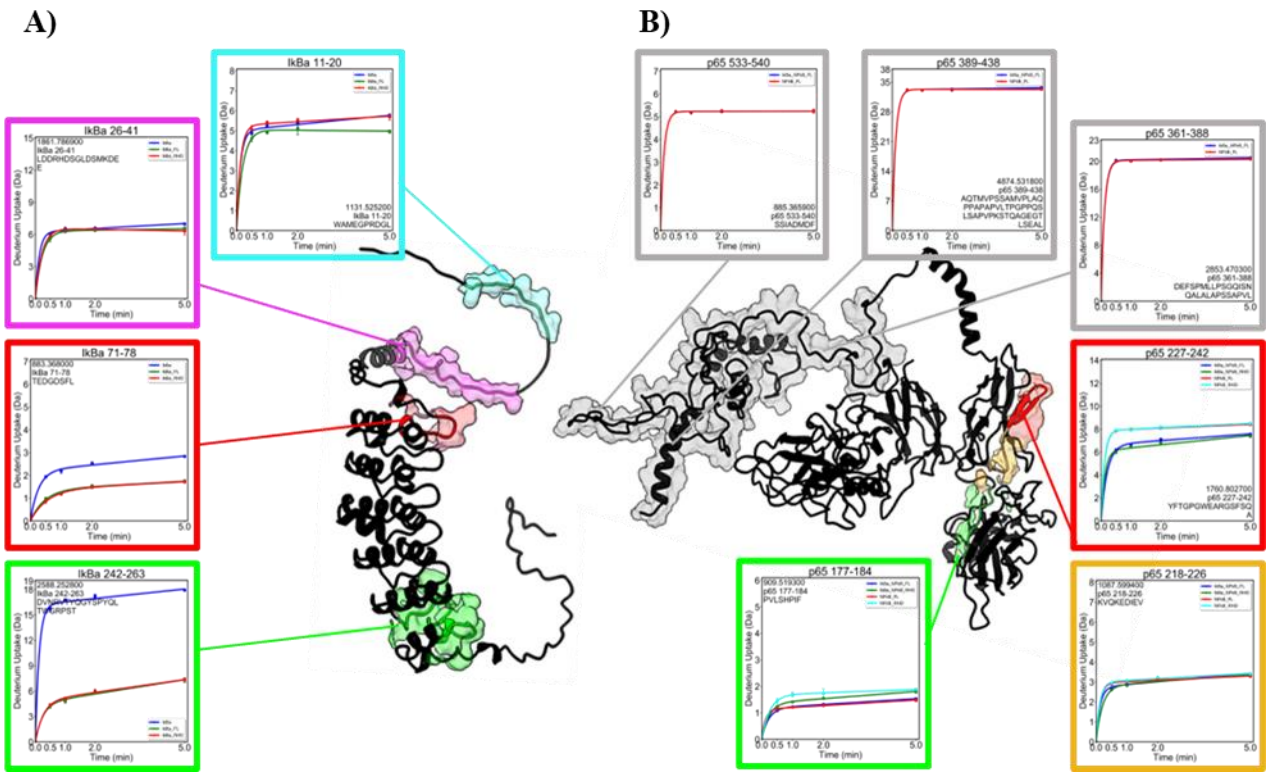

Figure 7 HDX-MS uptake plots of IκBα and NFκB unbound vs bound

The NFκB is either $NFkB_{RHD}$ or $NFkB_{FL}$. A) Structure of IκBα with the corresponding HDX uptake plots for the protein unbound vs bound to $NFkB_{RHD}$ or $NFkB_{FL}$. In blue and pink are the regions of IκBα that had previously not been characterized and pink corresponds specifically to the peptides containing S32 and S36. Red indicates the region of IκBα that is a known binding hotspot. Green is a known region of IκBα that exhibits disorder-to-order. B) Structure of $NFkB_{FL}$ and the corresponding HDX-MS uptake plots for both $NFkB_{RHD}$ and $NFkB_{FL}$unbound vs bound to IκBα. In grey are the regions of NFκB previously not characterized in the presence of IκBα. In red is a known binding hot spot between NFκB and IκBα. In green and yellow are regions found to be interesting in other studies performed.

Discussion

HDX-MS results indicate that the TAD in NFκB does not have any effect on the binding interface with its inhibitor, IκB. Both $NFkB_{FL}$ and $NFkB'_{RHD}s$ DNA binding domains bind to IκBα's AR1-AR6 as previously observed. AR5 and AR6 exhibit the same level of disorder-to-order upon binding to NFκB . In contrast to previous belief (Röder and Wales 2018), the N-

terminus of IκBα remains disordered upon binding to NFκB as demonstrated by HDX-MS data. Regions highlighted in blue and pink (Fig. 7) do not capture a change in disorder-to-order upon binding. NFκB 's transcription activation domain appears to remain disordered upon binding to its inhibitor. These results determine that IκBα's disordered N-terminus and NFκB 's disordered C-terminus domain remains consistent across apo and bound states.

Chapter 3 FPOP: IkappaBalpha N-terminal Phosphorylation Sites Become Protected Upon Binding NFkappaB

3.1 FPOP Introduction

Fast photochemical oxidation of proteins (FPOP) coupled with mass spectrometry is a powerful method that can be used across a large array of applications for protein foot-printing. This method has been extended to determine drug binding, epitope maps, and *in vitro/cell/vivo* protein structures (Yan, Chen et al. 2014, Li, Shi et al. 2018, Li and Chen 2019, Espino, King et al. 2020, Johnson, Punshon-Smith et al. 2020). Experiments presented here extend this method to characterize intrinsically disordered protein interactions.

3.1.1 Protein Foot-printing

When deconvoluting the synergy of multi-protein complexes such as the Nuclear Factor-kB Family (NFκB) there is a large array of methods that can be used for protein foot-printing; however, only few are compatible with the complexity of this system. While X-ray crystallography and CryoEM are limited by their inability to define intrinsically disordered regions (IDRs), conventional methods for studying IDRs such as NMR require significant effort for resonance assignments(Cornwell, Radford et al. 2018, McKenzie-Coe, Shortt et al. 2021). Mass Spectrometry (MS)-based protein foot-printing methods overcome these limitations. Hydrogen Deuterium Exchange Mass Spectrometry (HDX-MS) has proven to be a well-established method to characterize the interfaces and dynamics of biomolecular interactions. Another protein foot-printing method, Fast Photochemical Oxidation of Proteins (FPOP), takes advantage of the promiscuity of hydroxyl radicals, and its ability to interact with proteins, to label solvent accessible amino acids. FPOP coupled with MS is a promising technique given that its irreversible label broadens the capabilities of applying protein foot-printing methods on multi-protein complexes both in vitro and in cell.

3.1.2 Fundamentals of FPOP

Hydroxy radical based foot-printing was initially utilized to identify DNA binding sites, since hydroxyl radicals break DNA backbone that are solvent exposed. Tullius and Dombrowski's method of using Fenton chemistry to create hydroxy radicals and identify DNA-protein interactions (Tullius and Dombroski 1986, Ermácora, Delfino et al. 1992) paved the way for Hambly and Gross to extend this method as a means to probe the higher order of protein structure using the photochemical oxidation of proteins (FPOP) reaction (Hambly and Gross 2005). This application eventually led to the development of protein structure determination both *in cell* and *in vivo* by Espino and Jones (Espino, Mali et al. 2015).

Much like HDX, FPOP is a chemical approach that takes advantage of a compound with waterlike properties and high reactivity to probe the solvent exposed regions of proteins (27). When in solution, 19 of the 20 amino acids can theoretically react with hydroxyl radicals and form a covalent interaction which can be detected using mass spectrometry. Each amino acid has a different reactivity rate and different possible modifications that can be detected as mass change (Table 1). Sulfur containing amino acids are the most reactive, while glycine is the least reactive among the 20 natural amino acids; in fact, mass changes of glycine cannot be detected.

An early concern from this method was preserving the integrity of protein structures when labeling with hydroxyl radicals due to any steric or direct impact a hydroxy group could cause to the protein structure. However, the conditions of the experimental set up for *in vitro* FPOP have been tuned to provide structural information of proteins in their native conformation. Enzymatic activity of lysozyme was observed to be preserved after FPOP when limiting labeling efficiency to 30% of the protein and quenching the reaction under a microsecond time scale using glutamine followed by an absolute quench reaction with methionine and catalase.

Table 1 **FPOP Amino Acid Reactivity and Modifications.**

This table contains a row of residues with columns containing their one letter code, their corresponding reaction rate at neutral pH with hydroxyl radicals, and a row of modifications made along with their mass change in units of Dalton.

Residue	Code	Rate (M-1 S-1)	Modification Mass Change (Da)
Cys	C	3.50E+10	Sulfuric acid (+48), sulfuric acid (+32), hydroxy (-16)
Trp	W	1.30E+10	hydroxy- (+16, +16, +32, +48), pyrrol ring open (+32)
Tyr	Y	1.30E+10	hydroxy- (+16, +32)
Met	M	8.50E+9	sulfoxide (+16), sulfone (+32), aldehyde (-32)
Phe	F	6.90E+9	hydroxy- (+16, +32)
His	H	4.80E+9	Oxo- (+16), ring open (-22, -10, +5)
Arg	R	3.50E+9	hydroxy- (+16), deguanidination (-40), hydroxy- (+16), carbonyl (+14)
Ilg	I	1.80E+9	hydroxy- (+16), carbonyl (+14)
Leu	L	1.70E+9	hydroxy- (+16), carbonyl (+14)
Val	V	8.50E+8	hydroxy- (+16), carbonyl (+14)
Pro	P	6.50E+8	hydroxy- (+16), carbonyl (+14)
Gln	Q	5.40E+8	hydroxy- (+16), carbonyl (+14)
Thr	T	5.10E+8	hydroxy- (+16), carbonyl (-2- or +16-H20)
Lys	K	3.50E+8	hydroxy- (+16), carbonyl (+14)
Ser	S	3.20E+8	hydroxy- (+16), carbonyl (-2- or +16-H2O)
Glu	E	2.30E+8	hydroxy- (+16), decarboxylation (-30), carbonyl (+14)
Ala	A	7.70E+07	hydroxy- (+16)
Asp	D	7.50E+07	hydroxy- (+16), decarboxylation (-30)
Asn	N	4.90E+07	hydroxy- (+16)
Gly	G	1.70E+07	

Figure 8 In Vitro FPOP Workflow

A)

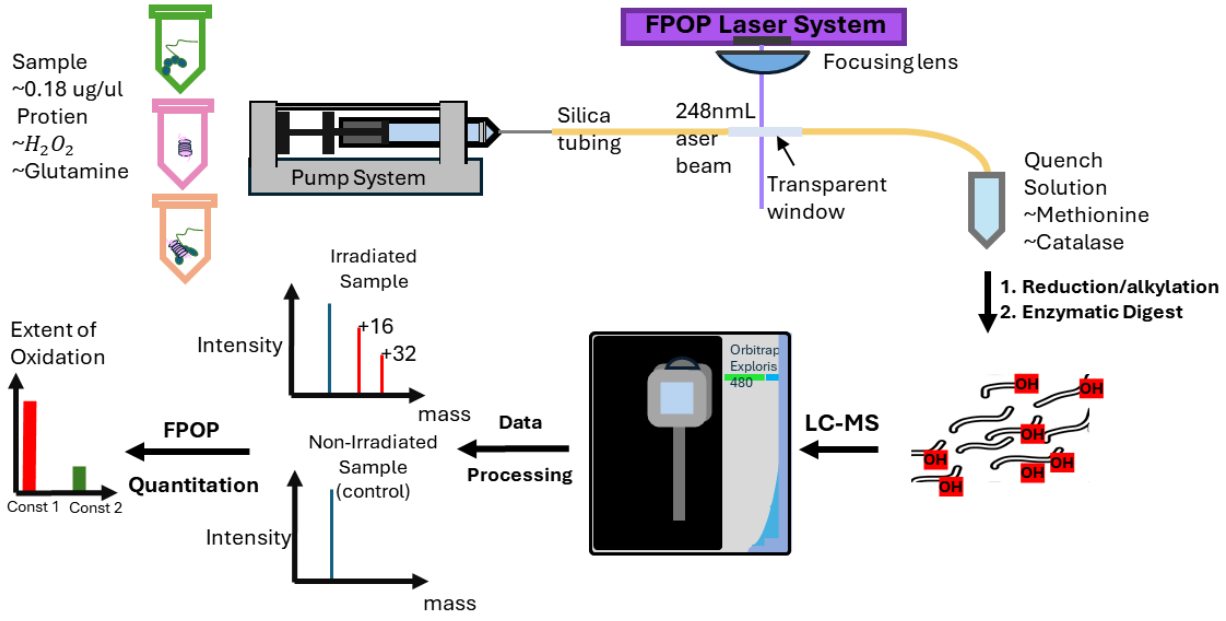

B)

$$Fe^{2+} + H_2O_2 \rightarrow Fe^{3+} + -OH + \cdot OH$$

Figure 8 In-Vitro FPOP starting from the sample preparation step.

Initially a sample is mixed with H_2O_2, and glutamine. This sample is then pumped with a syringe system into a silica tubing that is irradiated by a KrF_2 excimer laser and quenched in a solution containing methionine and catalase. The proteins are reduced, alkylated, and digested in preparation for LC-MS/MS analysis. The data is processed using Proteome Discover followed by a quantitative analysis that allows us to determine the extent of oxidation a peptide has received.

3.2 Methods

3.2.1 Sample Preparation for In Vitro FPOP

PBS buffer was made with 50mM Phosphate and 150mM NaCl. The following reagents were purchased from Fisher Chemical; L-glutamine, L-methionine, catalase, acetonitrile (ACN), hydrogen peroxide, acetone, 0.1% FA in wáter, 0.1% FA in ACN. The following kits were purchased from Fisher Scientific; Pierce Trypsin Protease MS-Grade 5 x 20 µg (90057), Pierce Universal Nuclease for Cell Lysis 5kU, 20 µl (88700), Mass Spec Sample Prep Kit for Culture Cells (8484700) (containing Digestion buffer, cell lysis buffer, dithiothreitol (DTT), and Iodoacetamide (IAA)). Mass spectrometry grade water was used to prepare buffer A (0.1% formic acid) and buffer B (acetonitrile with 0.1%) from Thermofisher.

The FPOP laser system used a 100 µl Hamilton syringe coupled to a fused silica tubing (Polymicro Technologies, Pheonix, AZ, USA) with 360 µm outer diameter (OD) and 150 µm inner diameter (ID). A transparent window is created by burning the coating of the silica tubing using a lighter until the silica tubing is clear, leaving the remaining glass.

The proteins were purified as described in chapter 3. Samples were stored at 4 ˚C until undergoing the FPOP reaction. When initiating the FPOP reaction, a 45 µL sample containing 0.18 µg/µL protein and 40 mM glutamine, was mixed with 5 µL 75 mM H2O2 (with a final concentration of 7.5 mM in the FPOP reaction) was vortexed, centrifuged, aspirated by a 100 µL syringe, and pumped into a silica tubing at a flow rate of 33.8 µl/min. Sample was irradiated by a KrF eximer laser (GAM Laser Inc, Orlando, FL, USA) with the following properties: frequency of 10 Hz and wavelength of 248 nm. Each condition had a total of five negative controls (not irradiated/ no laser) as well as five FPOP experimental replicates (irradiated/ laser). To guarantee consistency, the reactions for all conditions were prepared and executed on the

same day with the same stocks. Samples were then digested using an adapted protocol from Pierce Mass Spec Sample Prep Kit for Culture Cells, Document 2522. Samples were centrifuged for 10 minutes at 16,000 under a temperature of 4 ˚C. 10mM DTT was used to reduce disulfide bonds during a 45-minute incubation at 50 ˚C in a water bath. The sample was then cooled for 10 minutes, and thiol groups were alkylated with 50 mM IAA for 20 minutes at RT wrapped in aluminum foil in order to remain in a dark environment. The sample was then mixed with 460 µL of pre-chilled 100% acetone and allowed to precipitate overnight at -20 ˚C. The sample was centrifuged for 10 minutes at 16,000x g and supernatant was removed. The pallet was washed with 50 µl of 90% pre-chilled acetone and centrifuged for 5 minutes at 16,000 x g. After removal of remaining acetone, pallets were air dried for 3 minutes and resuspended in 100 µL of Pierce digestion buffer. Trypsin was added in a 1:20 ratio of enzyme to protein (based on starting protein concentration determined by nanodrop) and incubated overnight at 37 ˚C. The digestion reaction was quenched by creating a final concentration of 5% formic acid. Peptides were dried using a speed vacuum SC11- with refrigerated condensation trap in conjunction with a dual seal pump and resuspended with 30 µL of 0.1% FA.

3.2.2 Liquid Chromatography-Tandem Mass Spectrometry (LC-MS/MS)

Protein digest was loaded on Evotip C18 by following the Evosep sample loading protocol for Evotips. Dry C18 resin was washed with 20 µl solvent B and centrifuged at 700 x g for 60 seconds. The C18 resin tips were then conditioned by allowing the resin to soak in 100 µl 1-propanol until tips turned white. 20 µl of Solvent A was used to equilibrate soaked tips, followed by a 60 second centrifugation at 700 x g for two cycles. 20 µl of the protein digest was then loaded onto the wet tips. The C18 resin containing peptides was washed by adding 20 µl

solvent A and centrifuged for 60 seconds T 700 g. To keep the C18 resin wet, 100 µl of solvent A was added and centrifuged at 700 x g at 10 s.

Peptide separation was achieved using the manufacturers provided 44-minute gradient. Mass Spectrometry analysis was performed on an Exploris480. The acquisition parameters were as follows: data dependent acquisition mode, a mass spectrum with a scan range of 375-1200 m/z, with the resolution set to 120000, an intensity threshold of 8.0e3 was applied, with a charge state range of 2-6. Peptide fragmentation was accomplished using 30% HCD collision energy, and AGC target was customized to 30 % normalized AGC target, with an auto maximum injection time mode, 1 micro-scan, a profile a data type and polarity set to zero.

3.2.1 Data Analysis

Mass Spectrometry data were processed using Proteome Discover 2.2 (Thermo Fisher Scientific, Waltham, MA) using the Sequest algorithm. The following filtering parameters were applied to exclude low confidence peptides; tolerance for fragment ion was set to 0.02 Da, precursor ion tolerance was set to 10 ppm, enzyme specificity was set to trypsin, and peptides with false discovery rate above 5% were excluded. Data was further processed with Excel PowerPivot add-in customized to identify extent of modification for each peptide in which the sum of the area modified peptide is divided by the corresponding sum of the area of unmodified peptide (Rinas, Espino et al. 2016).

3.3 Results

3.3. 2 Trypsin Vs Chymotrypsin digest

The overall sequence coverage across all three conditions is shown in Figure 9A, the regions of the sequence that are not covered are missing tryptic cleavage sites.

Figure 9 In Vitro FPOP Sequence Coverage Map of IκBα.

A) The IκBα sequence is written with green bars below to represent tryptic peptide sequence coverage. The green blocks do no represent peptides but rather consolidated sequence coverage.

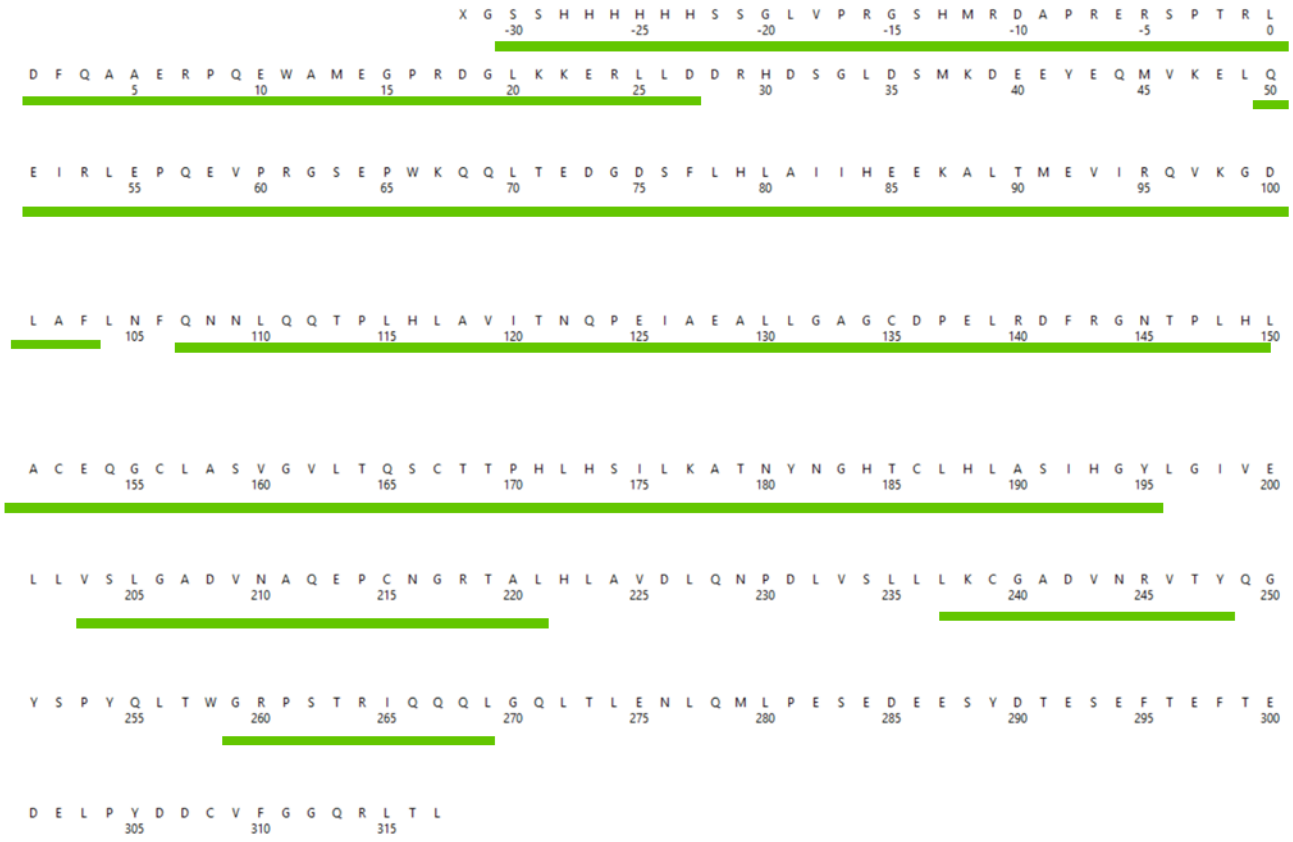

Figure 10 In Vitro FPOP Cymotrypsin Sequence Coverage Map of IκBα.

A) The IκBα sequence is sritten with green bars below to represent chymotryptic peptide sequence coverage.

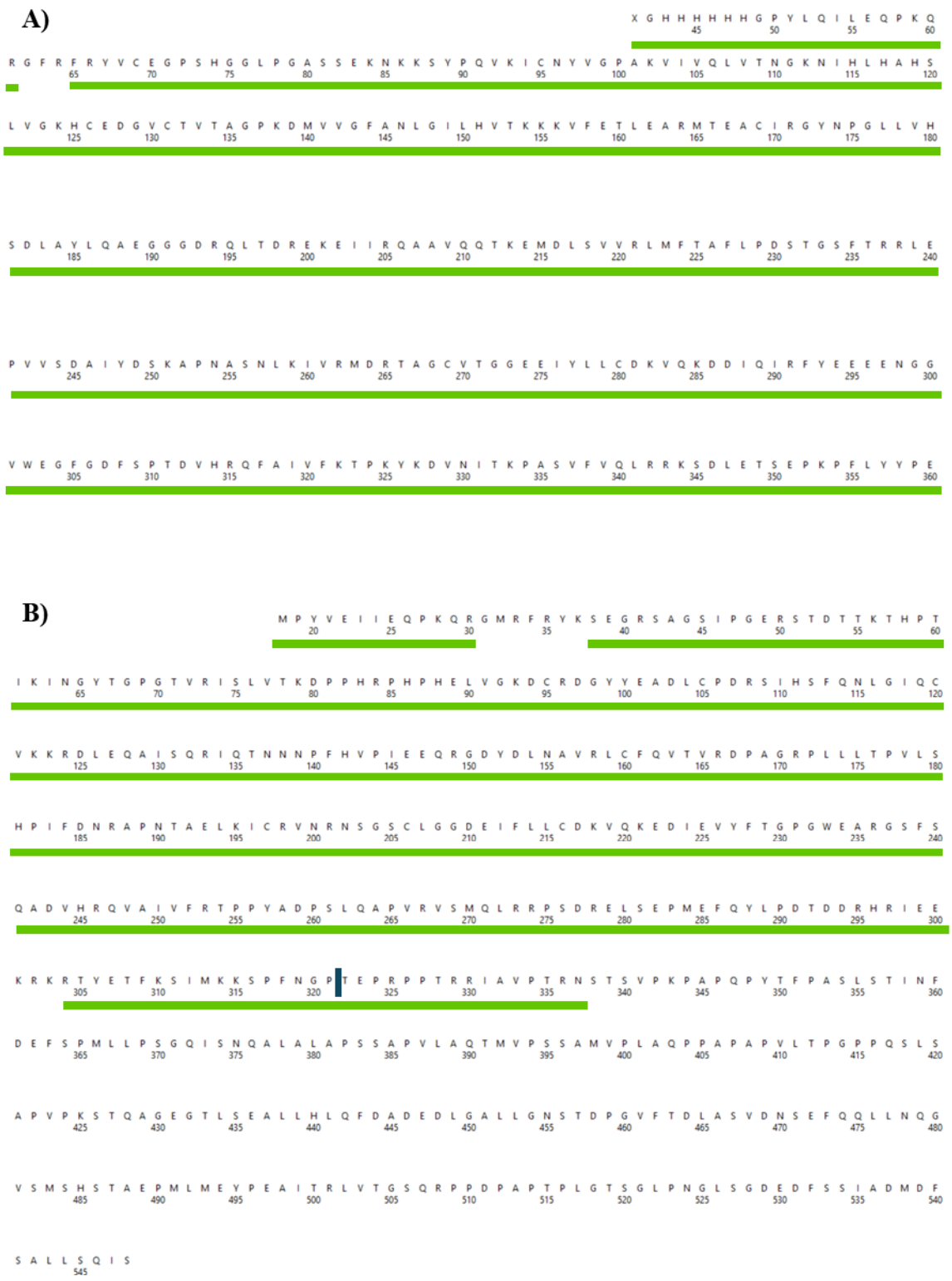

Figure 11 In Vitro FPOP Tryptic Sequence Coverage Map NFKB p50p65

A) The NFκB P50 sequence is sritten with green bars below to represent tryptic peptide sequence coverage. B) The NFkN p65 sequence is sritten with green bars below to represent tryptic peptide sequence coverage.

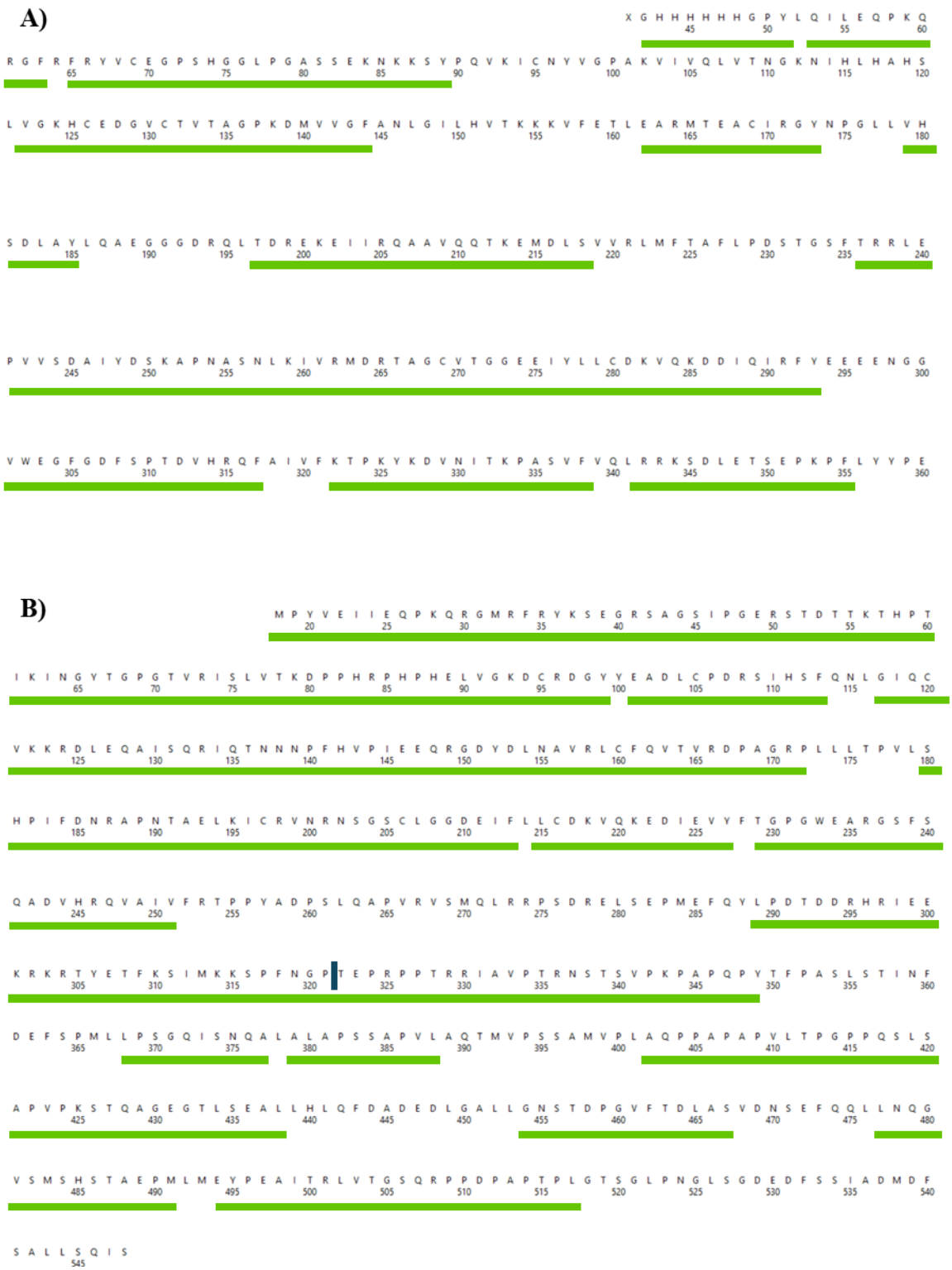

Figure 12 In Vitro FPOP Chymotryptic Sequence Coverage Map NFKB p50p65

A) The NFκB P50 sequence is sritten with green bars below to represent chymotryptic peptide sequence coverage. B) The NFkN p65 sequence is sritten with green bars below to represent chymotryptic peptide sequence coverage.

In-Vitro FPOP

Insert a page worth of text explaining how we got to these graphs. Give some evaluative statements. How many were initially there and how many were removed. If they drop out where do they drop out. And so on.

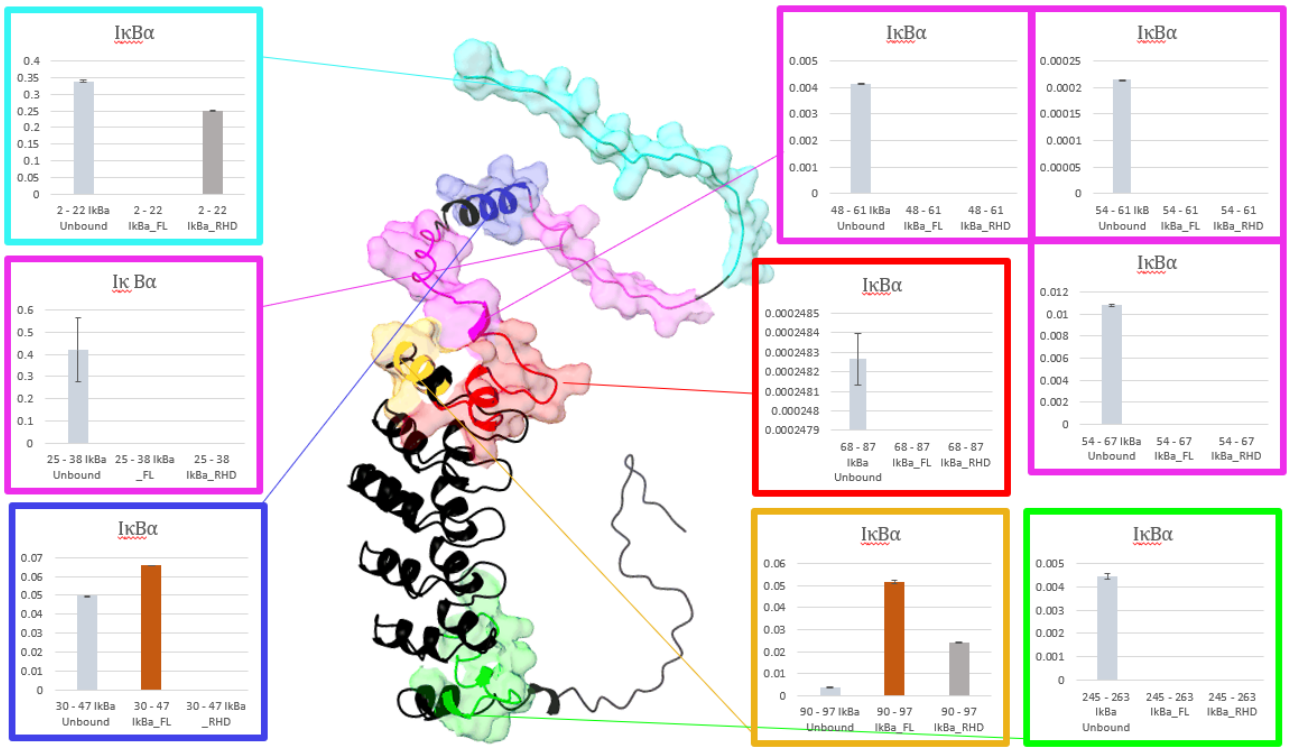

Figure 13 In Vitro Trypsin FPOP for IκBα

Bar graphs showing the ratio of oxidized to unoxidized peptide for each of the samples. Samples where there is no bar had significant amounts of unoxidized peptide, but no oxidized peptides were observed. The peptides in pink boxes were completely protected upon binding (i.e. no oxidized peptides were observed in the bound samples), the side chains of the peptides in the red box demonstrate the protection of known binding regions, the side chains of the peptides in blue boxes are only accessible under an apo and FL bound condition, the side chains of the peptides in a gold box re only accessible when bound to FL, and the amino acids in the peptides within a green box are showing the regions of NFκB that fold upon binding

A)

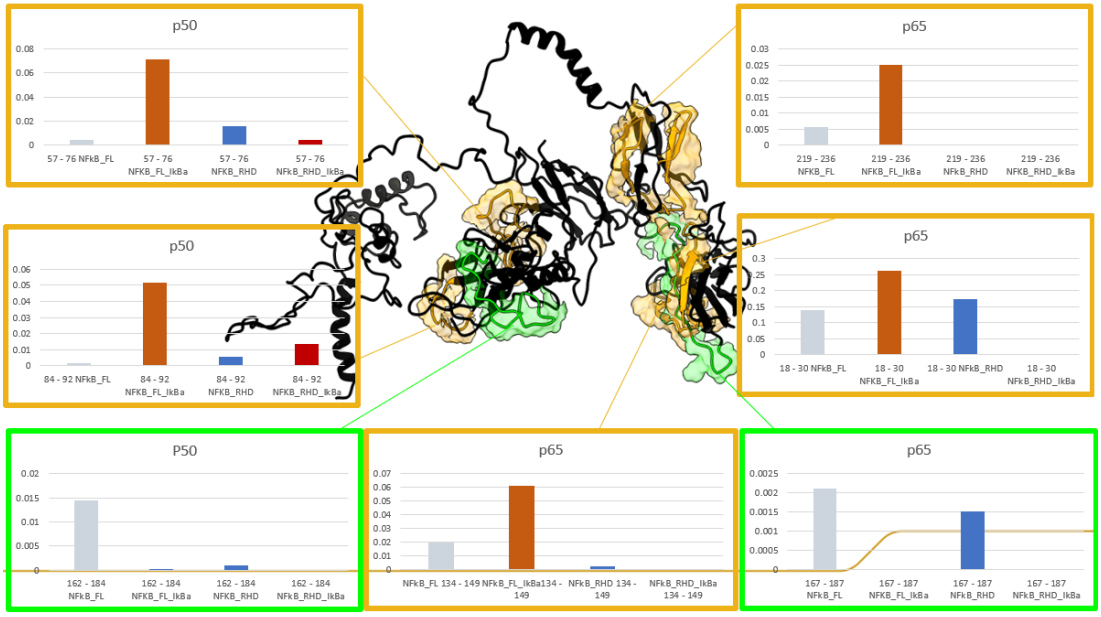

B)

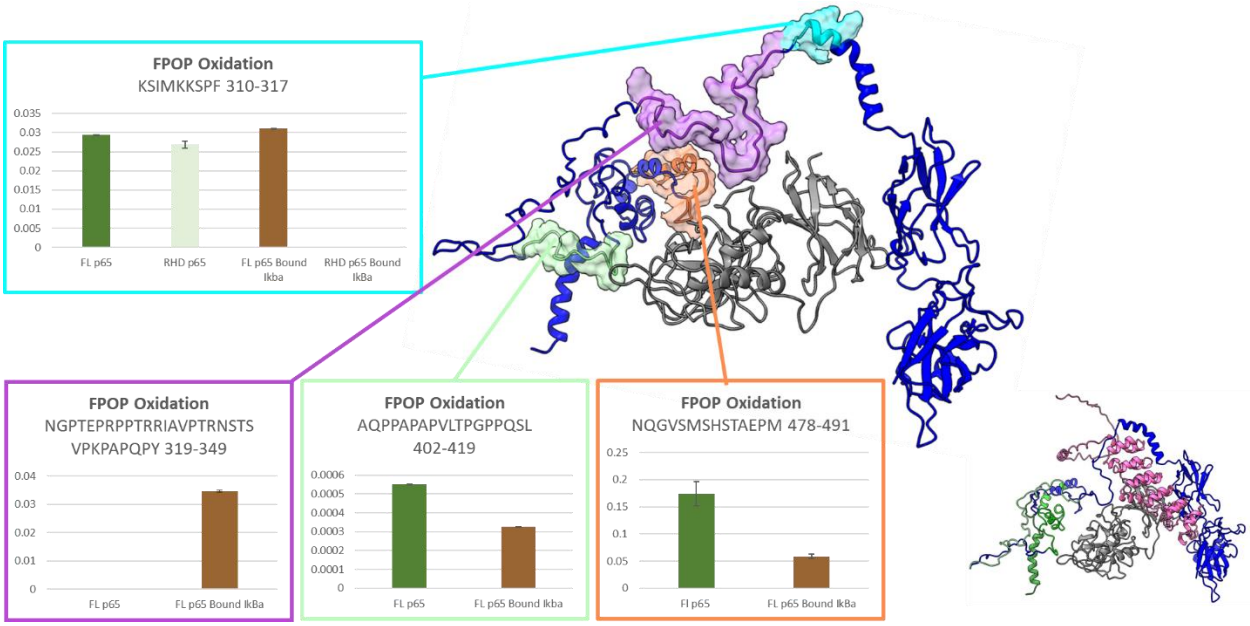

Figure 14 FPOP-MS results for NFκB p50RelA

A) FPOP Trypsin digest results. The side chains of the peptides in a green box demonstrate the protection of known hot spots upon binding, and the side chains of the peptides in gold boxes are most accessible when bound to FL. B) FPOP Chymotrypsin digest results.

FPOP-MS was performed to characterize the intrinsically disordered N-terminus of IκBα and the intrinsically disordered C-terminus of NFκB apo vs bound. I hypothesized that structural information of the intrinsically disordered regions may be captured by FPOP-MS experiments. The experiment will extend the application of FPOP-MS to characterize intrinsically disordered protein patterns such as the transition of disorder-to-order and elucidate any side chain interactions. FPOP-MS results capture the transition of disorder-to-order that occurs in AR6 of IκBα as highlighted in green, and the binding hotspot at AR1; in fact, regions of AR1 seems to be more protected when bound to NFκB _FL than when bound to the NFκB _RHD. N-terminal side chains in residues highlighted in pink are more protected when bound to NFκB _FL and NFκB _RHD, while N-terminal side chains highlighted in baby blue are most protected when bound to NFκB _FL and N-terminal side chains highlighted in navy blue are most protected when bound to NFκB _RHD (Fig. 11). FPOP-MS results capture regions of the DNA binding domain highlighted in green that are protected upon binding IκBα. Regions highlighted in gold show a decrease in protection within NFκB _FL when bound to IκBα in contrast to other conditions (NFκB _FL, NFκB _RHD and IκBα-NFκB _RHD).

Discussion

IDRs in proteins leverage the characteristics of flexibility and versatile dynamicity to maintain precise control over the regulation of signaling cascades. Regions that are recognized as signaling checkpoints like PTM sites, degron domains, Motifs, or LIMs are poorly characterized due to their universal characteristic of disorder. Here we use FPOP-MS to demonstrate a previously stated mechanism of disorder-to-order that occurs at IκBα's AR6 where its degron

region is located, and a binding hotspot at AR1. This experiment also identified protection that occur within IκBα's disordered N-terminal region when bound to NFκB . IκBα's N-terminal region which contains S32 and S36 that become phosphorylated by the IκBα kinase. Side chains of NFκB's TAD become protected when bound to IκBα, which leads us to believe that the N-terminus forms a fuzzy complex with NFκB's TAD. Further studies must be conducted to depict the exact mechanism that is occurring. Given the HDX-MS results presented in Chapter 2 along with FPOP-MS results presented in Chapter 3, we speculate that these side chain interactions are intramolecular and do not cause secondary structure formation. This mechanism could serve the purpose of increasing localized frustration (discussed in chapter 3) to destabilize this region to promote downstream degradation upon phosphorylation.

Chapter 4 Protein Frustration Analysis: IkappaBalpha's N-terminal Phosphorylation Sites Increase in Highly Frustrated Contacts Upon Binding NFkappaB

4.1 Background

The interaction between NFκB and IκBα is a central checkpoint of NFκB regulation. Despite previous advancements in the investigation of this tertiary complex, little is known about the IDRs and the energetic forces that promote both activation and inhibition of NFκB . Unveiling the biophysical characteristics of the IDRs of this complex may assist to further develop our understanding of NFκB regulation. In this chapter, a computational study was conducted to apply the physical concept of frustration to understand the synergetic characteristics that facilitate motion within these proteins and give rise to protein-protein interactions and protein folding.

Cyrus Levinthal believed that protein folding followed a random search until it found a "correct way to fold" which was recognized as the Levinthal paradox. This paradox would entail that all possible polypeptide conformations are equally probable and would eventually result in a native structure. However, proteins generally fold in timescales under milliseconds, which makes the above paradox improbable. Levinthal's solution to this paradox was that there must be "kinetic control" leading this protein folding through a 'narrower' pathway. Along with Levinthal's Paradox, protein folding in the 20th century was interpreted with phenomenological models such as the nucleation growth mechanism, the diffusion-collision model, the framework model, and the jigsaw-puzzle model. With recent advancements in computational and experimental approaches, the field now studies protein folding by characterizing the energetic properties that govern the physical constraints that bias the pathway of protein folding. This approach evolved to Bryngelson and Wolynes' development of a statistical model that leveraged the concept of frustration in the context of spin glass theories to define the principle of minimum frustration.

The mathematical code that derives the principle of minimum frustration was developed because the paradoxical characteristics of the phenomenological models developed to explain protein folding paralleled those of the statistical mechanics in glass/glasses transitions. By incorporating theories from glass physics in a coarse-grained Hamiltonian model, the kinetics of protein folding gave rise to a state in which secondary and tertiary structural features do not conflict with each other but rather reach minimal frustration. To reach a minimally frustrated state, energetic properties of each amino acid come into play in the context of the interactions that occur along the polypeptide both within geometric proximity and allosterically (Bryngelson and Wolynes 1987). The principle of minimal frustration led to the development of theoretical methods to perform local frustration calculations. Gonzalo Parra, Ferreiro, and Wolynes developed an open access web server that can be used to assign local frustration index scores that quantitate the extent of which a single residue can affect the overall energy of a structure in comparison to a decoy model that perturbs the local environment and generates frustration index scores. To generate mutational frustration index scores, *i* and *j* are defined as residues in which *i* and *j* are independently mutated in a pairwise function (when analyzing *i* only *j* is mutation, and vice versa) to the 20 most common amino acids giving rise to a simultaneous mutation analysis that generates a "mutational frustration" value (Fig 17 A). When generating configurational frustration values, the amino acid is perturbed beyond its identity. By displacing the location of each amino acid, the favorability of the native pair wise interaction can be determined relative to any additional pair-wise interactions which could be formed (Figure 17 B) (Parra, Schafer et al. 2016). This *in silico* analysis can be used to study and define the surface synergy that drives interactions, and disordered-to-ordered transitions that occur in tertiary complexes. By defining the localized highly frustrated contacts identified across different conditions, coarse grained models can be used to

investigate interactions that occur in regions that are highly disordered throughout the NFκB -IκBα complex.

A)

$$F_{ij}^{m} = \frac{\mathrm{E}_{\mathrm{i,j}}^{\mathrm{T,N}} - < E_{i',j'}^{T,U} >}{\sqrt{\frac{1}{N}\sum_{k=1}^{n}(E_{i',j'}^{T,U} - < e_{i',j'}^{T,U} >)^2}}$$

$\boldsymbol{E^{T,N}}$: total energy of the protein in its native configuration
$\boldsymbol{E^{T,U}}$: average energy of the decoys

B)

$$F_{ij}^{C} = \frac{\mathrm{E}_{\mathrm{i,j}}^{\mathrm{N}} - < E_{i',j'}^{U} >}{\sqrt{\frac{1}{N}\sum_{k=1}^{n}(E_{i',j'}^{U} - < e_{i',j'}^{U} >)^2}}$$

$\boldsymbol{E^{N}}$: Energy of a native contact of the protein in its native configuration
$\boldsymbol{E^{U}}$: average energy of randomly interacting sets within a molten globule

Figure 15 Protein Structure Perturbation Frustration Calculation

A) The equation that is used to derive the mutational frustration index scores is written above. The corresponding definitions of the variables are indicated below the equation. B) The equation that is used to derive the configurational frustration index scores is written above. The corresponding definitions of the variables are indicated below the equation.

4.2 Methods

4.2.1 Protein Preparation

To create an accurate *in silico* NFκB ($p65_{(19-550)}$)-IκB$\alpha_{(2-317)}$ PDB protein structure, a series of standard procedures to create models of IDPs was first completed, and then the proteins were equilibrated/relaxed (Fig. 11).The structure of the NFκB ($p65_{(19-321)}$)-IκB$\alpha_{(67-317)}$ complex were used from a crystal structure (Huxford, Huang et al. 1998), while the structure for the NFκB ($p65_{(19-550)}$) construct was taken from an unbound model generated using AWSEM and SAXS data (Baughman, Narang et al. 2022). The structure for IκB$\alpha_{(2-317)}$ was generated using AlphaFold. First, NFκB ($p65_{(19-550)}$) residues 322-550 were stitched onto the NFκB p($65_{(19-321)}$)-IκB$\alpha_{(67-31)}$ using Modeller. This generated a model with NFκB ($p65_{(19-550)}$)-IκB$\alpha_{(67-31)}$. Then IκB$\alpha_{(2-317)\ was}$ docked onto NFκB ($p65_{(19-550)}$) by aligning IκB$\alpha_{(2-317)}$ and IκB$\alpha_{(67-31)}$ using PyMol. This allowed us to generate a structure for the NFκB p($65_{(19-550)}$)-IκB$\alpha_{(2-317)}$ complex. Hereon IκB$\alpha_{(2-317)}$ will be referred to as IκBα, and NFκB ($p65_{(19-550)}$), NFκB ($p65_{(19-321)}$) will be referred to as NFκB $_{FL}$, and NFκB $_{RHD}$ respectively. Constructs were prepared by following recommendations from Amber relaxation tutorial found at https://ambermd.org/tutorials/basic/tutorial13/index.php

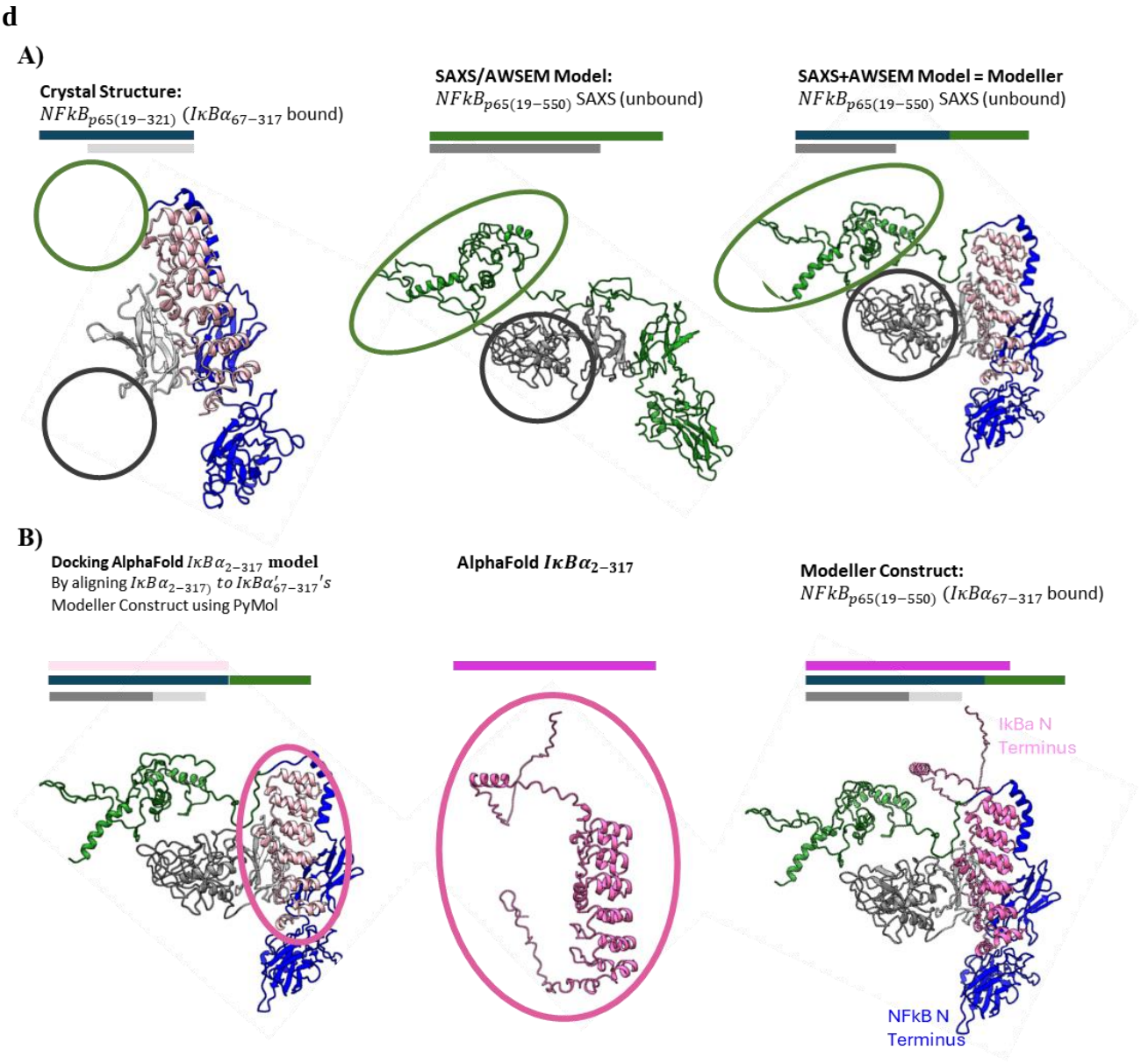

Figure 16 Model Building Steps followed to create an NFκB $_{FL}$-IκBα structure.

A) An illustration of the steps taken to prepare the NFκB $_{FL}$-IκBα structure from previously validated domains. Here the crystal structure obtained from the protein data bank as 1IKN (truncated NFκB bound to truncated IκBα) is illustrated in blue, the full length NFκB structure obtained from an AWSEM IDP and SAXS experiments is illustrated in green. Full length IκBα was obtained using AlphaFold. B) Is a snapshot of the system that will relaxed and equilibrated after protonation and solvation of the system. C) Once the system is ready, the amber tutorial for relaxing and equilibrating a system were followed to reach a stable equilibrated state prior to a Frustratometer analysis.

3.2.2 Frustratometer

An open-source software, http://frustratometer.qb.fcen.uba.ar/, was used to identify highly frustrated contacts via mutational perturbation and configurational perturbation. After acquiring highly frustrated contact index scores from configurational perturbations, the data was exported, and converted into csv files. Different conditions were then processed on Microsoft Excel to calculate the change in highly frustrated contacts because of hFrustration Index scores. hFrustration Index Scores of apo protein was subtracted from hFrustration Index Scores to calculate the change in frustration, which we will now refer to as Δ(hFrus). The workflow for this procedure was repeated for all constructs of interest: IκBα$_{(2-317)}$, NFκB $_{FL}$, NFκB $_{RHD}$, IκBα$_{(2-317)}$-NFκB $_{FL}$, and IκBα$_{(2-317-}$NFκB $_{RHD}$. Δ(hFrus) were then plotted on a scatter plot to visualize variabilities across different constructs (Fig 12).

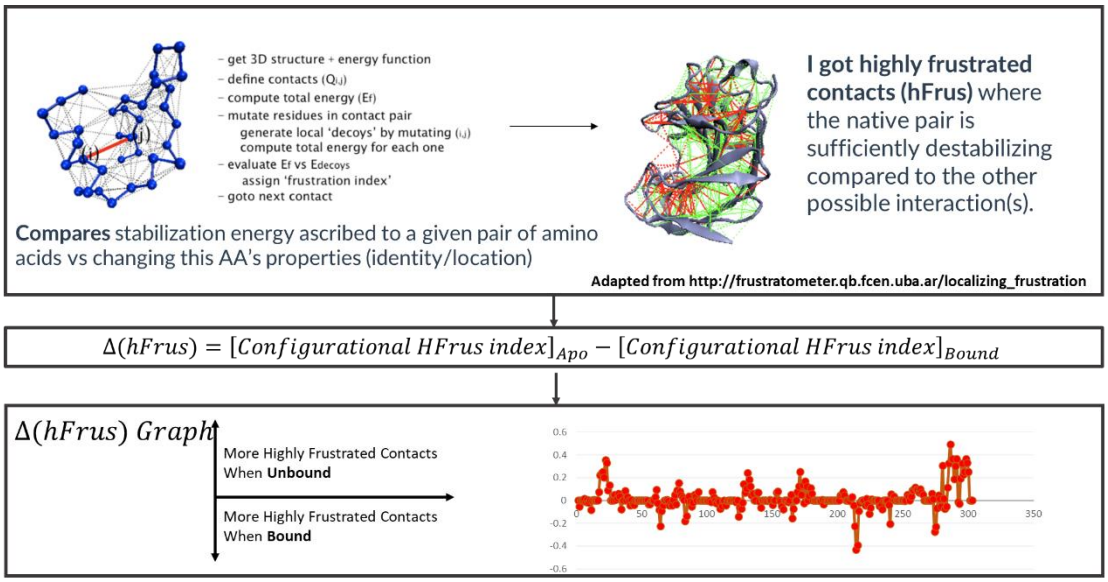

Figure 17 Workflow to generate change in highly frustrated contacts

Frustratometer Workflow illustration adapted from http://frustratometer.qb.fcen.uba.ar/localizing_frustration uses a 3D structure and the energy function to compare stabilization energy ascribed to a given pair of amino acids by changing the amino acid identity and/or location. From this, the highly frustrated contacts Δ(hFrust) were identified where the native pair is sufficiently destabilizing compared to the other possible identities.

4.3 Results

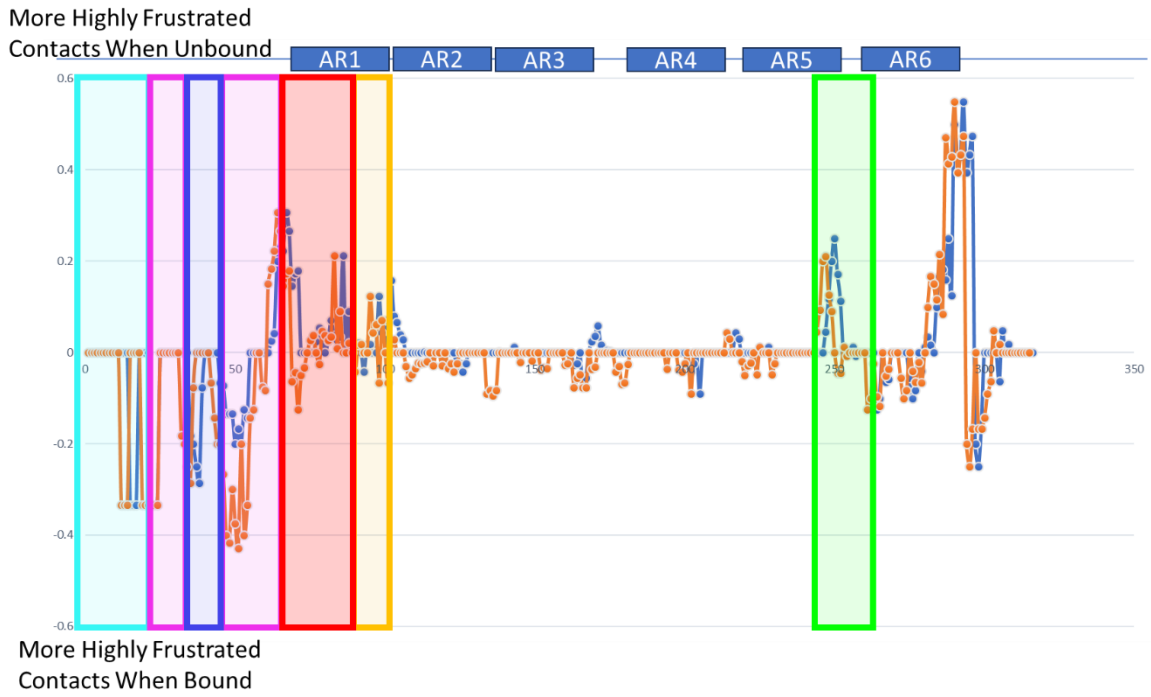

Figure 18 Δ(hFrust) of IκBα bound to NFκB RHD vs bound to NFκB Fl.

The graph above is two scatter plots overlayed in which the x axis is the residue number of IκBα and the y axis is the calculated Δ(hFrust) of IκBα when bound to NFκB $_{FL}$ in blue and NFκB $_{RHD}$ in orange. The boxes highlight regions that can be matched with experimental data in chapters 2 and 3.

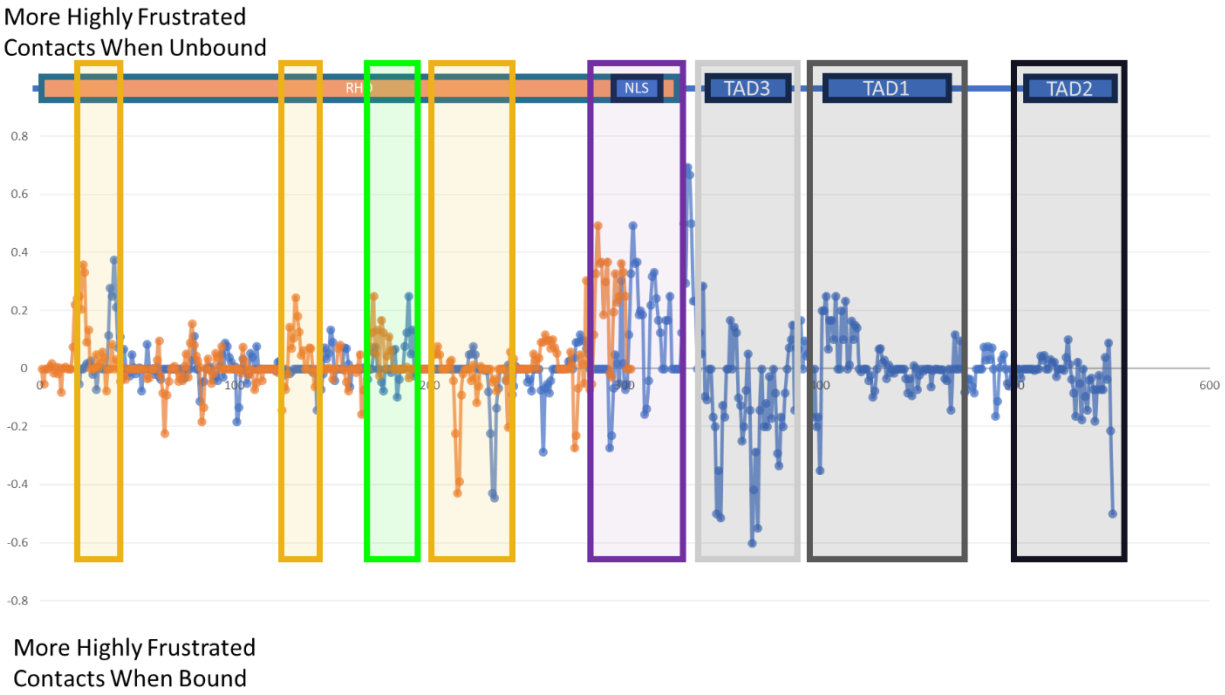

Figure 19 Δ(hFrust) of NFκB RHD bound to IκBα vs NFκB Fl bound to IκBα.

The graph above is two scatter plots overlayed in which the x axis is the residue number of NFκB $_{p65}$ and the y axis the calculated Δ(hFrust) of NFκB $_{FL}$ in blue and NFκB $_{RHD}$ in oange. The boxes highlight regions that can be matched with experimental data in chapters 2 and 3.

Discussion

This in silico analysis identified more highly frustrated contacts within IκBα's AR5 and AR6 apo vs bound to NFκB . This result corroborates with the HDX-MS and FPOP-MS results that were presented in chapter 2 and chapter 3. The ability of this in-silico analysis to identify a decrease in highly frustrated contacts upon exhibiting a disordered-to-ordered transitions led us to believe this would aid in investigating the intrinsically disordered regions of IκBα and NFκB. Frustratometer also allowed us to localize amino acids that may undergo transient interactions intra/intermolecularly when the protein forms a tertiary complex. The configurational frustration analysis on the NFκB - IκBα tertiary complex captures highly frustrated contacts in both disordered and ordered regions of a this protein complex which help tie in characteristics captured with HDX-MS and FPOP-MS. FPOP-MS. While HDX-MS results identified that the integrity of IκBα's N terminal domain remains the same apo vs bound, FPOP-MS and Frustratometer capture IκBa's N-terminal side chains near phosphorylation sites S32 and S36 are protected upon binding to NFκB both $NF\kappa B_{FL}$ and $NF\kappa B_{RHD}$. Here, Frustration analysis shows this region becomes more highly frustrated upon NFκB binding demonstrating an increase in highly frustrated contacts detected by Frustratometer while maintaining disorder according to HDX-MS findings. HDX-MS did not capture any change in disorder throughout NFκB's TAD. FPOP MS does identify the possibility of a fuzzy complex forming between IκBα's signal recognition domain (N-terminus) and NFκB's TAD. The NLS becomes less frustrated upon binding to IκBα. The TAD becomes more frustrated upon binding IκBα as identified by an increase in frustrated contacts within TA3 and TA2 when bound to IκBα, and a decrease in frustrated contacts within TA1 upon binding.

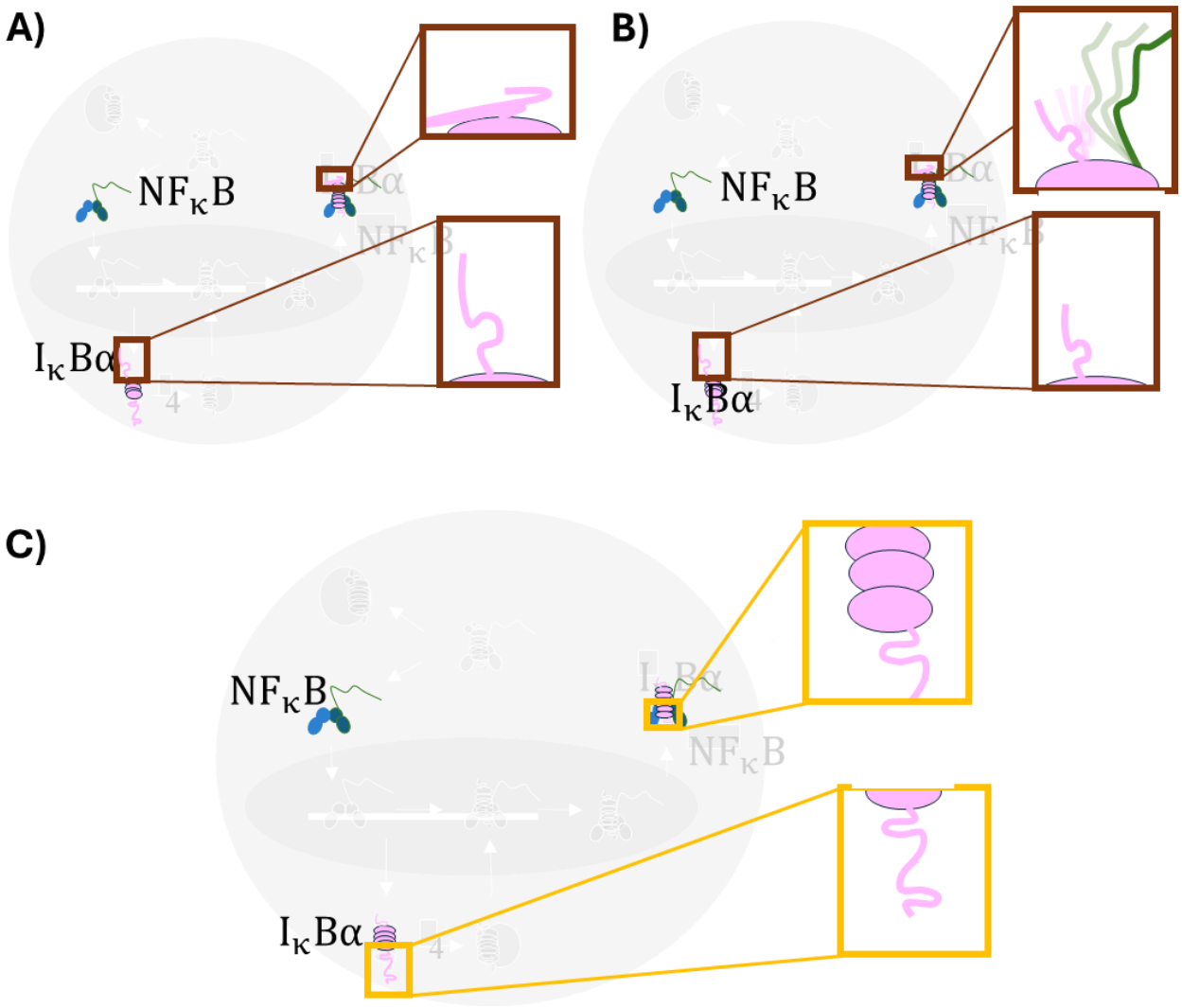

Figure 20 Proposed Mechanisms from Biophysical Characterizations

A) Illustrates the proposed mechanism of what may be occurring in the IκBα-NFκB (RHD) conditions. The N terminal domain seems to become protected upon the side chain interface but not the backbone interface. B) The transcription activation domain of NFκB and the N terminal domain of IκBα appear to be transiently interacting according to FPOP and frustratometer. However, HDX does not capture any back bone protection occurring, which could entail that the regions remain disordered and are transiently interacting with each other via inter-molecular side chain interactions. This is illustrated by the green line being the NFκB TAD and the pink line being the IκBα N terminus domain. These domains are drawn bouncing off of each other. C) The known mechanism of disordered-to-ordered transition in AR5 and AR6 is a well established mechanism, here FPOP, HDX-MS and frustratometer are all used to capture this phenomenon.

Acknowledgements

Chapter 1, 2, 3, and 4 contain material that will be used for publication by the author of this thesis.

REFERENCES

Baughman, H. E. R., D. Narang, W. Chen, A. C. Villagrán Suárez, J. Lee, M. J. Bachochin, T. R. Gunther, P. G. Wolynes and E. A. Komives (2022). "An intrinsically disordered transcription activation domain increases the DNA binding affinity and reduces the specificity of NFκB p50/RelA." Journal of Biological Chemistry **298**(9): 102349.

Bellucci, A., L. Bubacco, F. Longhena, E. Parrella, G. Faustini, V. Porrini, F. Bono, C. Missale and M. Pizzi (2020). "Nuclear Factor-κB Dysregulation and α-Synuclein Pathology: Critical Interplay in the Pathogenesis of Parkinson's Disease." Frontiers in Aging Neuroscience **12**.

Bryngelson, J. D. and P. G. Wolynes (1987). "Spin glasses and the statistical mechanics of protein folding." Proceedings of the National Academy of Sciences **84**(21): 7524-7528.

Cornwell, O., S. E. Radford, A. E. Ashcroft and J. R. Ault (2018). "Comparing Hydrogen Deuterium Exchange and Fast Photochemical Oxidation of Proteins: a Structural Characterisation of Wild-Type and ΔN6 β₂-Microglobulin." Journal of the American Society for Mass Spectrometry **29**(12): 2413-2426.

Davis, M., A. Hatzubai, J. S. Andersen, E. Ben-Shushan, G. Z. Fisher, A. Yaron, A. Bauskin, F. Mercurio, M. Mann and Y. Ben-Neriah (2002). "Pseudosubstrate regulation of the SCF^{β-TrCP} ubiquitin ligase by hnRNP-U." Genes & Development **16**(4): 439-451.

Dixit, V. and T. W. Mak (2002). "NFκB Signaling." Cell **111**(5): 615-619.

Ermácora, M. R., J. M. Delfino, B. Cuenoud, A. Schepartz and R. O. Fox (1992). "Conformation-dependent cleavage of staphylococcal nuclease with a disulfide-linked iron chelate." Proceedings of the National Academy of Sciences **89**(14): 6383-6387.

Espino, J. A., C. D. King, L. M. Jones and R. A. S. Robinson (2020). "In Vivo Fast Photochemical Oxidation of Proteins Using Enhanced Multiplexing Proteomics." Analytical Chemistry **92**(11): 7596-7603.

Espino, J. A., V. S. Mali and L. M. Jones (2015). "In Cell Footprinting Coupled with Mass Spectrometry for the Structural Analysis of Proteins in Live Cells." Analytical Chemistry **87**(15): 7971-7978.

Hambly, D. M. and M. L. Gross (2005). "Laser flash photolysis of hydrogen peroxide to oxidize protein solvent-accessible residues on the microsecond timescale." Journal of the American Society for Mass Spectrometry **16**(12): 2057-2063.

Huxford, T., D.-B. Huang, S. Malek and G. Ghosh (1998). "The Crystal Structure of the IκBα/NFκB Complex Reveals Mechanisms of NFκB Inactivation." Cell **95**(6): 759-770.

Johnson, D. T., B. Punshon-Smith, J. A. Espino, A. Gershenson and L. M. Jones (2020). "Implementing In-Cell Fast Photochemical Oxidation of Proteins in a Platform Incubator with a Movable XY Stage." Analytical Chemistry **92**(2): 1691-1696.

Lecoq, L., L. Raiola, P. R. Chabot, N. Cyr, G. Arseneault, P. Legault and J. G. Omichinski (2017). "Structural characterization of interactions between transactivation domain 1 of the p65 subunit of NFκB and transcription regulatory factors." Nucleic Acids Research **45**(9): 5564-5576.

Li, J. and G. Chen (2019). "The use of fast photochemical oxidation of proteins coupled with mass spectrometry in protein therapeutics discovery and development." Drug Discovery Today **24**(3): 829-834.

Li, K. S., L. Shi and M. L. Gross (2018). "Mass Spectrometry-Based Fast Photochemical Oxidation of Proteins (FPOP) for Higher Order Structure Characterization." Accounts of Chemical Research **51**(3): 736-744.

Liu, T., L. Zhang, D. Joo and S.-C. Sun (2017). "NFκB signaling in inflammation." Signal Transduction and Targeted Therapy **2**(1): 17023.

McKenzie-Coe, A., R. Shortt and L. M. Jones (2021). "THE MAKING OF A FOOTPRINT IN PROTEIN FOOTPRINTING: A REVIEW IN HONOR OF MICHAEL L. GROSS." Mass Spectrometry Reviews **40**(3): 177-200.

Parra, R. G., N. P. Schafer, L. G. Radusky, M.-Y. Tsai, A. B. Guzovsky, P. G. Wolynes and D. U. Ferreiro (2016). "Protein Frustratometer 2: a tool to localize energetic frustration in protein molecules, now with electrostatics." Nucleic Acids Research **44**(W1): W356-W360.

Rinas, A., J. A. Espino and L. M. Jones (2016). "An efficient quantitation strategy for hydroxyl radical-mediated protein footprinting using Proteome Discoverer." Analytical and Bioanalytical Chemistry **408**(11): 3021-3031.

Röder, K. and D. J. Wales (2018). "Evolved Minimal Frustration in Multifunctional Biomolecules." The Journal of Physical Chemistry B **122**(49): 10989-10995.

Sue, S.-C., C. Cervantes, E. A. Komives and H. J. Dyson (2008). "Transfer of Flexibility between Ankyrin Repeats in IκBα upon Formation of the NFκB Complex." Journal of Molecular Biology **380**(5): 917-931.

Taniguchi, K. and M. Karin (2018). "NFκB , inflammation, immunity and cancer: coming of age." Nature Reviews Immunology **18**(5): 309-324.

Tullius, T. D. and B. A. Dombroski (1986). "Hydroxyl radical "footprinting": high-resolution information about DNA-protein contacts and application to lambda repressor and Cro protein." Proceedings of the National Academy of Sciences **83**(15): 5469-5473.

Yan, Y., G. Chen, H. Wei, R. Y. C. Huang, J. Mo, D. L. Rempel, A. A. Tymiak and M. L. Gross (2014). "Fast Photochemical Oxidation of Proteins (FPOP) Maps the Epitope of EGFR Binding to Adnectin." Journal of the American Society for Mass Spectrometry **25**(12): 2084-2092.